Uwe Reisgen • Dietmar Drummer

Enhanced Material and Part Optimization and Process Intensification

Proceedings of the third International Joint Conference on
Enhanced Material and Part Optimization and Process Intensification EMPOrIA 2026
02nd and 03rd of June 2026, Aachen, Germany

Editors

Uwe Reisgen
RWTH Aachen University
Welding and Joining Institute
Germany

Dietmar Drummer
Friedrich-Alexander-Universität Erlangen-Nürnberg
Institute of Polymer Technology
Germany

Uwe Reisgen, Dietmar Drummer (eds.)

EMPOrIA 2026

Proceedings of the third International Joint Conference
on Enhanced Material and Part Optimization and
Process Intensification

Shaker Verlag
Düren 2026

Bibliographic information published by the Deutsche Nationalbibliothek
The Deutsche Nationalbibliothek lists this publication in the Deutsche Nationalbibliografie; detailed bibliographic data are available in the Internet at http://dnb.d-nb.de.

Shaker Verlag 2026

Print-ISBN 978-3-8191-0730-6
PDF-ISBN 978-3-8191-0670-5
https://doi.org/10.2370/9783819106705

Shaker Verlag GmbH • Am Langen Graben 15a • 52353 Düren
Phone: 0049/2421/99011-0 • Telefax: 0049/2421/99011-9
Internet: www.shaker.de • e-mail: info@shaker.de

Date: 13.03.2026

Narrowband aeroacoustic gas modulation for improved cut-edge quality in laser fusion cutting of austenitic stainless steels

Author: Marcelo de Oliveira Lopes[1]

Authors: Frank Schneider[2], Arnold Gillner[1], Constantin Häfner[3]

[1]RWTH Aachen University, Chair for Laser Technology, Steinbachstr. 15, 52074, AACHEN, GERMANY

[2]Fraunhofer Institute for Laser Technology, Steinbachstr. 15, 52074, AACHEN, GERMANY

[3]RWTH Aachen University, Templergraben 55, 52062 AACHEN, GERMANY

*Corresponding author: E-mail: marcelo.lopes@llt.rwth-aachen.de, ORCID: 0000-0003-0991-9016

Abstract

This paper summarizes fundamental studies of subproject A08 within SFB 1120 and addresses a limitation in laser fusion cutting of austenitic stainless steels: pronounced cut-edge roughness and burr formation, thereby constraining the process window. The presented approach introduces a resonator-equipped modulating nozzle (“cutting whistle”) that imposes a targeted narrowband aeroacoustic gas modulation to stabilize melt-film transport without increasing overall gas consumption. A reduced thin-film framework links gas-side interfacial shear and streamwise pressure gradients to blocking behavior and a film-side cutoff frequency, guiding frequency-band selection. The actuator provides a geometrically determined fundamental mode; modulation amplitude increases with stagnation pressure. High-speed imaging confirms a depth-dependent low-pass melt response, with lower and mid bands coupling more effectively into the exit region. Under matched throughput, narrowband modulation increases mean interfacial shear, stabilizes the melt transport, reduces roughness and burr in paired comparisons, and moderately increases the maximum cutting speed.

Keywords

laser fusion cutting, aeroacoustic modulation, melt-film stability, cut-edge roughness, austenitic stainless steel.

1 Introduction

Laser fusion cutting is widely used for manufacturing austenitic stainless steel components, offering high geometric flexibility and oxidation-free cut edges [1]. A persistent limitation, however, is pronounced cut-edge roughness and adherent burr, which constrain the usable process window in terms of feed rate, focus position, and gas pressure [2,3]. This becomes particularly

critical for sheet thicknesses above ~6 mm, where defects typically intensify toward the lower front region [4]. At the beginning of Collaborative Research Centre (SFB) 1120, roughness values of $R_z \approx 60–70$ µm with adherent burr were common for 6 mm stainless steel under industrial conditions. The long-term target is $R_z < 10$ µm with essentially burr-free edges.

Within SFB 1120, subproject A08 addresses this challenge through in-situ diagnosis and control of melt and solidification dynamics during laser fusion cutting, based on the hypothesis that the dominant quality limitations arise from insufficiently understood melt-front instabilities and their coupling to compressible gas flow. Accordingly, A08 follows an evolutionary approach: Phase 1 established a transparent trimming-cut test rig with high-speed imaging to directly observe melt-film motion and solidification, enabling experimental assessment of kerf multiple reflections [5,6] and demonstrating that controlled beam divergence can calm the melt stream and reduce instability-driven fluctuations [7]. In Phase 2, the diagnostic platform was expanded by schlieren imaging and acoustic measurements of the gas jet, revealing thickness-dependent resonances of the coupled gas–film system and motivating resonance-based actuation concepts [8]. Phase 3 consolidates these insights into process-compensation strategies using passive actuator-based modulation designed for compatibility with industrial cutting heads [9]. In this context, the present paper highlights a representative, industrially viable outcome: a resonator-equipped modulating nozzle ("cutting whistle") that superimposes a geometrically defined, narrowband aeroacoustic tone on the gas [10]. Building on a reduced thin-film framework, we relate this actuation to a depth-resolved melt response measured by high-speed imaging and to paired quality metrics (roughness, burr, maximum cutting speed) under matched gas throughput, thereby demonstrating how diagnostics-driven understanding and targeted actuation can increase cut-edge precision relative to the initial state at the start of SFB 1120.

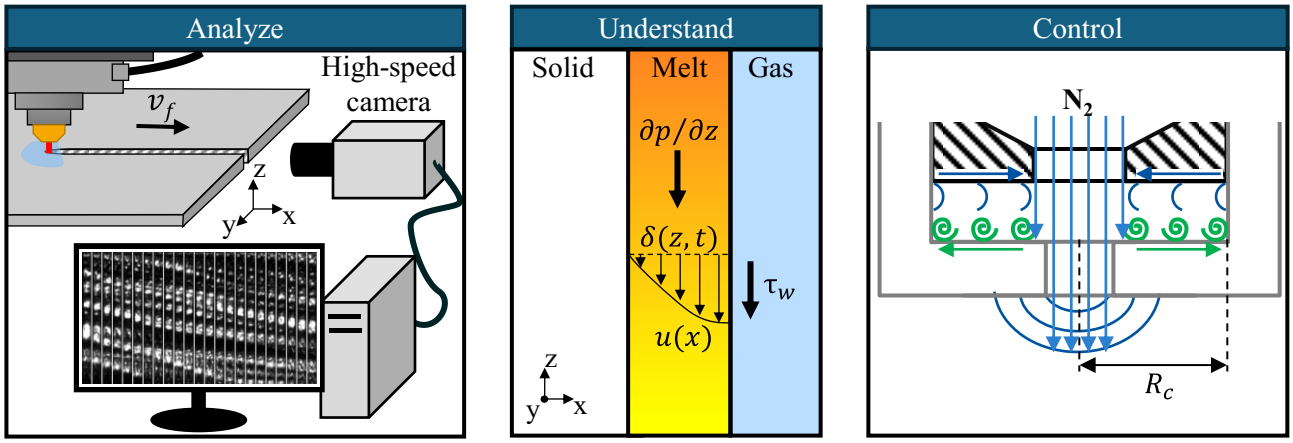

Figure 1: Methodological approach in SFB 1120: analyze–understand–control. In-situ process diagnostics quantify melt-film motion and gas–front interaction (Analyze). A reduced melt-flow framework interprets the dominant mechanisms and yields design-relevant guidance (Understand). Based on this, a resonator-equipped nozzle ("cutting whistle") is developed and applied to impose narrowband gas modulation that targets melt-film instabilities (Control).

2 Aim of the Investigation

The aim is to assess whether a resonator-equipped nozzle can stabilize melt evacuation near the lower front by imposing a depth-effective narrowband gas modulation without increasing gas

throughput. Specifically, we test whether band selection guided by a thin-film cutoff concept yields measurable reductions in lower-zone R_z and burr height H_{burr} in paired comparisons against a standard nozzle.

3 Materials and Experimental Details

Experiments were conducted on austenitic stainless steel (1.4301) sheets with thicknesses of 6 mm and 10 mm. Cutting was performed with a 1030 nm CW disk laser ($P_L = 6$ kW) using a Precitec HPSSL cutting head. The beam was delivered via a 100 µm fiber and shaped by 100 mm collimation and 200 mm focusing optics, resulting in an approximately 200 µm focus diameter. Focus position z_f and feed rate v_f were varied to span a representative process window, while comparisons between nozzle concepts were conducted under otherwise identical conditions. Nitrogen gas was supplied at stagnation pressures $p_0 = 12$–24 bar for cutting trials; additional 0–20 bar pressure ramps were used for actuator characterization. The gas was delivered coaxially through nozzles with 3 mm outlet diameter, comparing a standard conical nozzle against a resonator-equipped cutting whistle (variants A/B/C covering low-, mid-, and high-frequency bands). The nozzle stand-off N_z was adjustable and verified mechanically; the norm-volume flow Q_N was measured to enforce matched throughput in paired comparisons.

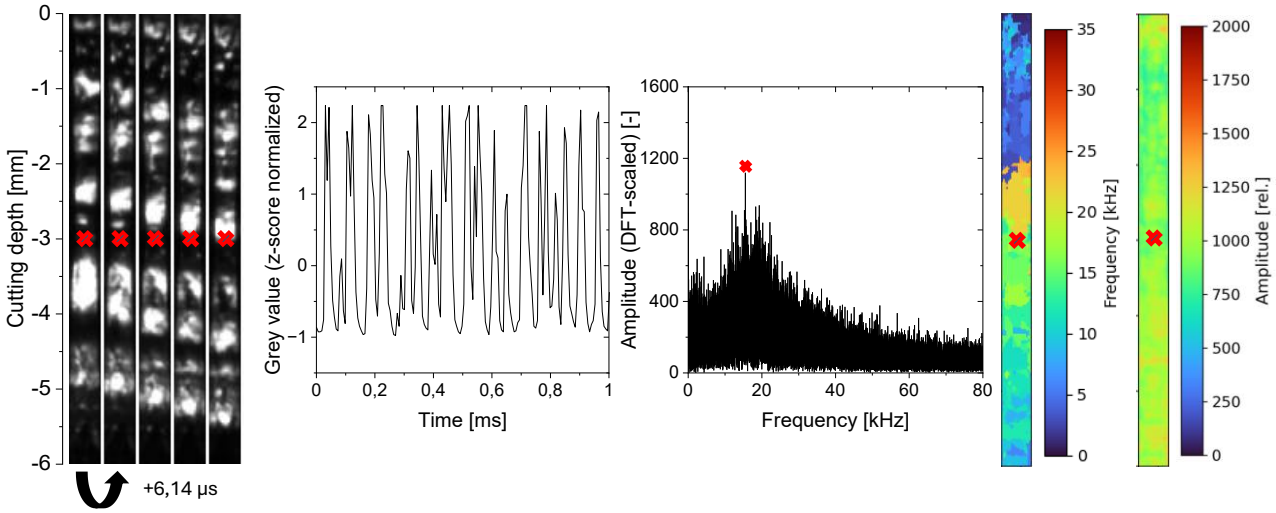

Figure 2: Pixel FFT pipeline for obtaining frequency-selective metrics. Left: z-normalized sample time series of a front pixel with dominant modulation. Right: corresponding amplitude spectrum with peak at and schematic derivation of frequency heatmaps and amplitude heatmaps.

Actuator behavior was quantified by microphone spectroscopy (STFT-based spectrograms/spectra for f_0, tonality, and pressure trends) and schlieren imaging of the gas jet in free jet and a transparent kerf model (coupling studies). Melt-front dynamics were captured by frontal high-speed imaging at approximately 1.6×10^5 fps, covering the full front depth from the top surface to the kerf exit. Pixelwise spectral analysis yielded dominant-frequency maps $f_{\mathrm{dom}}(y, z)$ and frequency-selective amplitude maps $A(y, z \mid f_0 \pm \Delta f)$ around the actuator fundamental; phase organization was evaluated using bandpass filtering around f_0, Hilbert-phase extraction, and phase-locking value (PLV) maps. Cut-edge quality was assessed under matched throughput by lower-zone roughness R_z (ISO 9013; optical profilometry at 1 mm above the lower edge), burr height H_{burr} (tactile

profilometry), and the maximum cutting speed $v_{f,\max}$ determined by feed-rate ramping to the last fully separating cut. Unless stated otherwise, results are reported from paired experiments (identical material, optics, p_0, N_z, and v_f), ensuring that differences in melt dynamics and quality are attributable to narrowband modulation rather than changes in average gas delivery.

4 Results and Discussion

4.1 Cutting whistle: schlieren- and acoustics-based results

The standard nozzle exhibits predominantly broadband acoustic emission with intermittently pressure-dependent bands appearing. Across the investigated pressure range, no single narrowband line can be tracked as a phase-stable fundamental mode. In contrast, all cutting-whistle variants (A/B/C) produce a pronounced narrowband fundamental mode with harmonic overtones. In pressure-ramp spectrograms this appears as a nearly vertical line whose amplitude increases with stagnation pressure, while its frequency remains essentially constant within the lock-in operating window. Any residual frequency variations are in the order of the spectral resolution and peak-fit uncertainty, i.e., no systematic pressure-induced frequency shift is observed in lock-in. For the representative mid-band configuration (Design B), the fundamental remains near $f_0 \approx 15$ kHz over the full investigated range (0–20 bar) (Fig. 3 (a)).

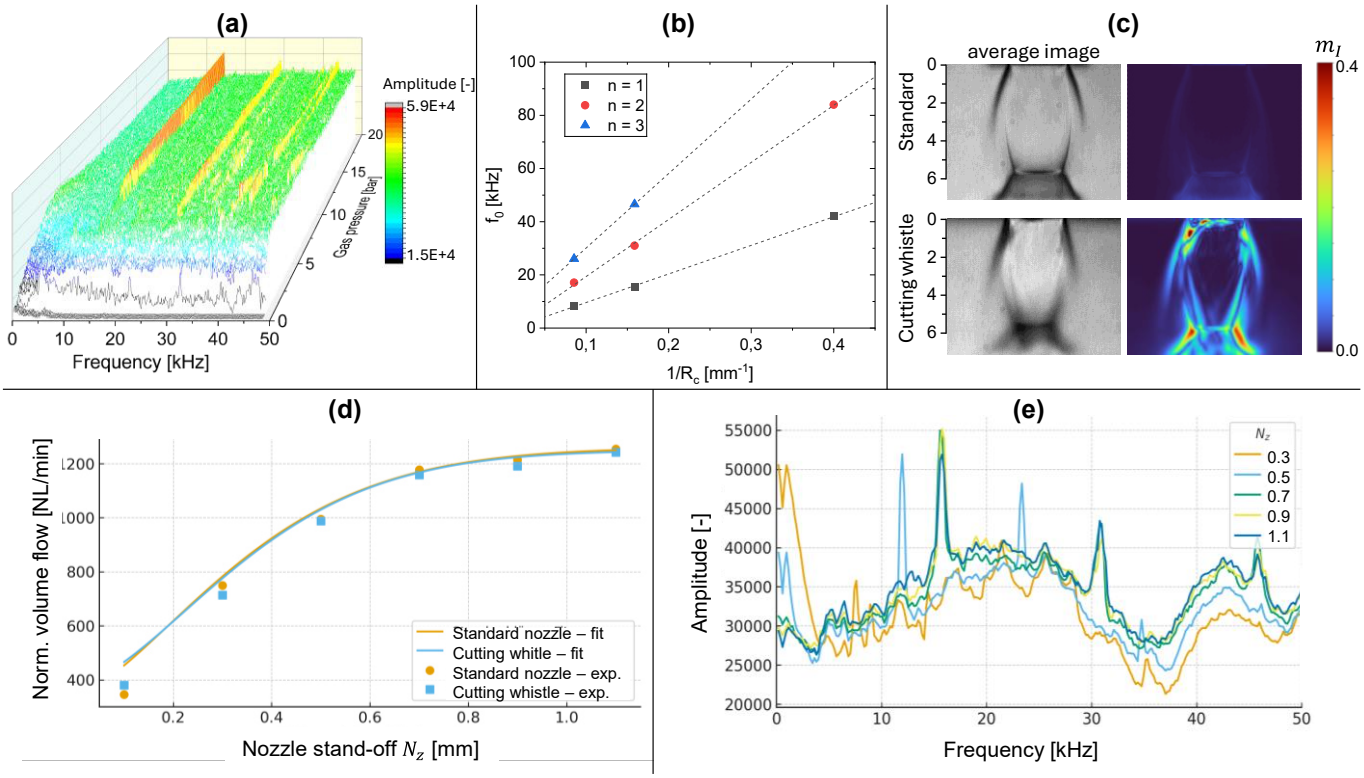

Figure 3: Cutting-whistle actuator characterization. (a) Pressure-ramp spectrogram showing a narrowband lock-in fundamental f_0 with amplitude increasing with p_0; (b) geometry scaling of f_0 versus $1/R_c$ (variants A–C); (c) time-averaged schlieren images and modulation-index maps m_I demonstrating coherent jet modulation for the cutting whistle (design B) compared to the standard nozzle; (d) norm-volume flow Q_N versus stand-off N_z indicating a hydraulic plateau near $N_z \approx 0.7$ mm; (e) microphone spectra for different nozzle stand-offs N_z(design B), illustrating lock-in near $f_0 \approx 15$ kHz for $N_z \geq 0.7$mm and detuning to lower bands at smaller N_z.

Across variants A–C, the fundamental frequency f_0 shifts systematically with cavity geometry and spans distinct excitation bands: A (low band, ≈ 8–17 kHz), B (mid band, ≈ 15–30 kHz), and C (high band, e.g., ≈ 40–80 kHz). When the lock-in-stable mean values of f_0 are plotted versus the inverse effective cavity radius $1/R_c$, the data follow a linear relationship (Fig. 3 (b)). This confirms the intended Rossiter/Strouhal-type geometry scaling [11]: larger cavity radii yield lower eigenfrequencies, smaller radii yield higher eigenfrequencies. Practically, this establishes a clear separation of roles: frequency selection is primarily geometric (A/B/C).

Schlieren imaging further demonstrates that the cutting whistle introduces a coherent narrowband modulation into the free jet that is absent for the standard nozzle (Fig. 3c). For the standard nozzle, schlieren sequences are dominated by broadband structures without a persistent narrowband corridor. For the cutting whistle (Design B), bandpass evaluation around f_0 yields a spatially connected modulation corridor in the near-field jet core. We quantify this effect by a schlieren-based modulation index $m_I = \hat{I}_{\mathrm{RMS}}/\bar{I}$, computed from the band-limited schlieren intensity fluctuations around f_0 and normalized by the local mean intensity. Although schlieren signals are not a direct velocity measurement, the band-limited intensity variations in the jet core scale with the strength of the coherent density-gradient structures associated with the imposed shear-layer mode; therefore m_I provides a conservative, dimensionless proxy of the relative modulation depth. Assuming $\hat{U}/\bar{U} \gtrsim m_I$ (lower-bound mapping), the quadratic dependence of wall shear on velocity implies a mean-shear increase $\Delta\bar{\tau}_w/\bar{\tau}_w \approx \frac{1}{2}(\hat{U}/\bar{U})^2 \gtrsim \frac{1}{2}m_I^2$. With $m_I \approx 0.2$–0.3 this yields $\Delta\bar{\tau}_w/\bar{\tau}_w \approx 2$–$4.5\%$ even under throughput parity, providing a mechanistic lever for stabilizing melt-film transport.

The nozzle stand-off N_z is shown to be the dominant coupling parameter between the modulated jet and the kerf entrance. Flow measurements at $p_0 = 20$ bar reveal a steep increase of $Q_N(N_z)$ at small stand-off and a clear approach to a plateau at larger N_z for both nozzle types (Fig. 3 (d)). Already at $N_z = 0.7$ mm both nozzles reach roughly 94 % of the plateau. Thus, increasing N_z beyond ~0.7 mm yields only marginal throughput gains out of the nozzle. Acoustically, N_z controls whether the cutting whistle operates in its intended lock-in band or becomes detuned (Fig. 3e). For $N_z \geq 0.7$ mm the dominant mode remains in the expected lock-in region around $f_0 \approx 15$ kHz and stays essentially constant, consistent with stable geometric resonance under hydraulically open conditions. At smaller distances, the system remains tonal but the dominant frequency shifts downward (≈12 kHz at $N_z = 0.5$ mm and ≈7 kHz at $N_z = 0.3$ mm), indicating detuned regimes linked to altered entrance impedance and inlet throttling. The Prominence Ratio PR is used here as a tonality metric, defined as the peak level at f_0 relative to a local broadband "mask" level around the peak (i.e., $PR = L_{\mathrm{peak}} - L_{\mathrm{mask}}$, where L_{mask} is obtained from locally smoothed spectral background). While PR can peak slightly near $N_z \approx 0.5$ mm, this primarily reflects a reduced broadband background; in the hydraulically open regime ($N_z \approx 0.7$ mm) the absolute tonal line amplitude is higher, but the broadband level is also higher, which reduces PR despite stronger

modulation. Overall, $N_z \approx 0.7$ mm provides the most robust operating point, combining near-full throughput with stable lock-in at the intended f_0 and strong tonal forcing.

4.2 Melt dynamics and reduced model: depth-resolved response to narrowband forcing

To interpret how a narrowband gas excitation translates into cut-edge quality, we employ a reduced thin-film framework in which the melt layer on the inclined cutting front is driven by two gas-side pathways: interfacial shear stress (Couette-type forcing) and a streamwise pressure gradient along the front (Poiseuille-type forcing) [12]. In this picture, stable evacuation requires that shear-driven transport remains sufficiently strong relative to locally adverse pressure forcing that would otherwise thicken the film and promote intermittent accumulation ("blocking-prone" behavior). Such adverse pressure forcing can arise locally when kerf coupling weakens or becomes non-uniform—for example due to jet spreading/leakage, or shock/boundary-layer interactions that impose spatially localized back-pressure regions along the front [13]. In the lower kerf, where the melt film is typically thicker and shear levels tend to decay, even modest local increases in streamwise pressure forcing or transient drops in interfacial shear can shift the film into a buildup/emptying regime rather than a global standstill. Linearizing the forced thin-film response yields a film-side cutoff frequency that separates effectively transmitted perturbations from strongly damped ones. In scaling form,

$$f_c \sim \frac{\bar{\tau}_w}{\eta_m \bar{\delta}},$$

where $\bar{\tau}_w$ denotes a representative mean shear stress, η_m an effective melt viscosity, and $\bar{\delta}$ an effective film thickness. Since $\bar{\tau}_w$ typically decreases and $\bar{\delta}$ tends to increase towards the kerf exit, the model predicts a depth-dependent low-pass behavior: higher-frequency forcing is increasingly filtered with depth, while lower-frequency forcing can penetrate further—provided the excitation remains at or below the local f_c of the target depth region.

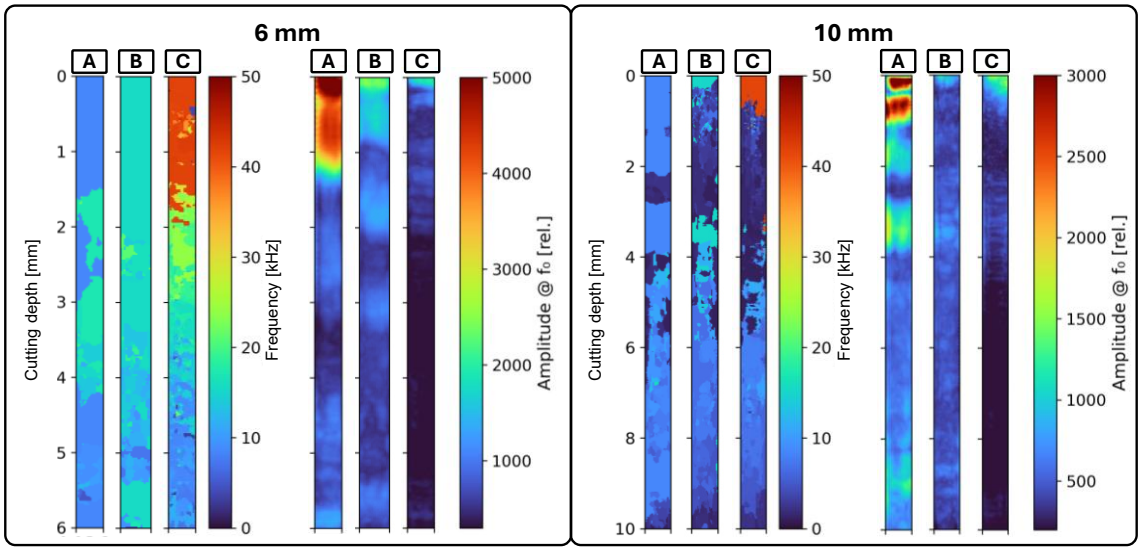

Figure 4: Depth-resolved melt response to cutting-whistle variants A/B/C at $p_0 = 20$ bar and $N_z = 0.7$ mm. $f_{\mathrm{dom}}(y,z)$ and $A(y,z \mid f_0 \pm \Delta f)$ show strong near-top response for all bands; low/mid bands penetrate deeper than the high band. Representative 10 mm cases indicate a downward shift of the depth-effective band.

The depth-resolved high-speed imaging results support these predictions (Fig. 4–5). For 6 mm stainless steel under representative conditions, the imposed fundamental is clearly visible in the upper front region for all cutting-whistle variants, including high-band excitation. With increasing depth, however, the response becomes strongly frequency selective: low and mid bands maintain a measurable signature deeper into the kerf, whereas the high band decays rapidly and remains largely confined to the upper portion. This trend is consistent with the depth-dependent low-pass filtering implied by $f_c(z)$. 10 mm datasets show the same hierarchy shifted toward lower effective bands: the deeply effective band moves to lower frequencies as thickness increases, in line with the expectation that $\bar{\delta}$ and/or η_m increase and thus reduce f_c.

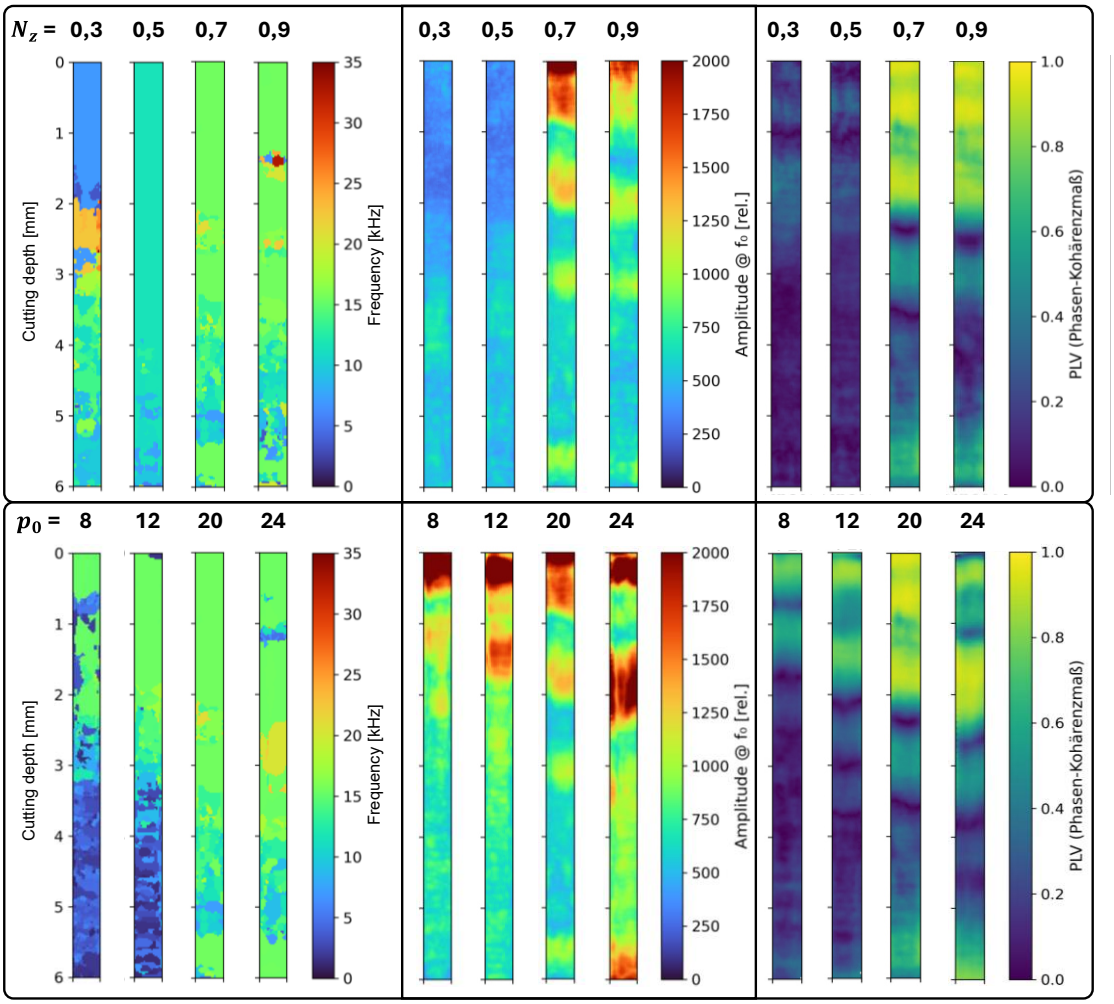

Figure 5: Lock-in and coupling trends for design B (6 mm): f_{dom}, $A(y,z \mid f_0)$, and PLV versus p_0 and N_z. Higher p_0 strengthens response and coherence; coupling is maximal near $N_z \approx 0.7$ mm, with detuning at small N_z.

Beyond amplitude trends, the measurements also confirm the model's operating-point dependence via pressure and stand-off. Increasing stagnation pressure strengthens the imposed modulation and, through the quadratic dependence of shear on velocity [14], increases the mean shear stress $\bar{\tau}_w$ [15], thereby widening the dynamic bandwidth and improving depth effectiveness. Correspondingly, coherence metrics (PLV) exhibit broader plateaus at higher pressures in the lock-in regime, indicating that the forced oscillation is not only detectable but remains phase-organized over a larger fraction of the front depth. The nozzle stand-off N_z acts as a coupling selector: at too

small N_z, the system detunes toward lower modes and the nominal excitation band couples less effectively; at too large N_z, jet spreading and leakage weaken the effective forcing. In the intermediate coupling window around $N_z \approx 0.7$ mm, both mode fidelity and coherence are maximized, which is consistent with the framework's requirement that a sufficiently strong and well-coupled shear forcing must be maintained to keep the melt film away from blocking-prone regimes near the exit.

Overall, the experiments corroborate the reduced framework in three key, design-relevant trends: (i) the cutting front behaves as a depth-dependent low-pass to narrowband forcing, (ii) frequency-band selection must target the exit region (i.e., $f_0 \lesssim f_c$ at the lower front), with the effective band shifting downward for larger thickness, and (iii) the depth effectiveness is controlled by operating point—notably stagnation pressure and stand-off—through their impact on mean shear and coupling efficiency.

4.3 Precision gains and process window

Across the full dataset of 70 paired parameter combinations (6 mm), the cutting whistle reduces lower-zone roughness R_z and burr height H_{burr} in the majority of operating points. In median, R_z decreases by ~18%, and in about four out of five paired cases the roughness with the cutting whistle is lower than with the standard nozzle. Burr height shows an even stronger improvement: the median reduction is ~33%, and approximately seven out of ten paired cases exhibit lower burr with the cutting whistle. These global trends indicate that the imposed narrowband modulation is not a marginal effect confined to isolated parameter points, but a reproducible process lever.

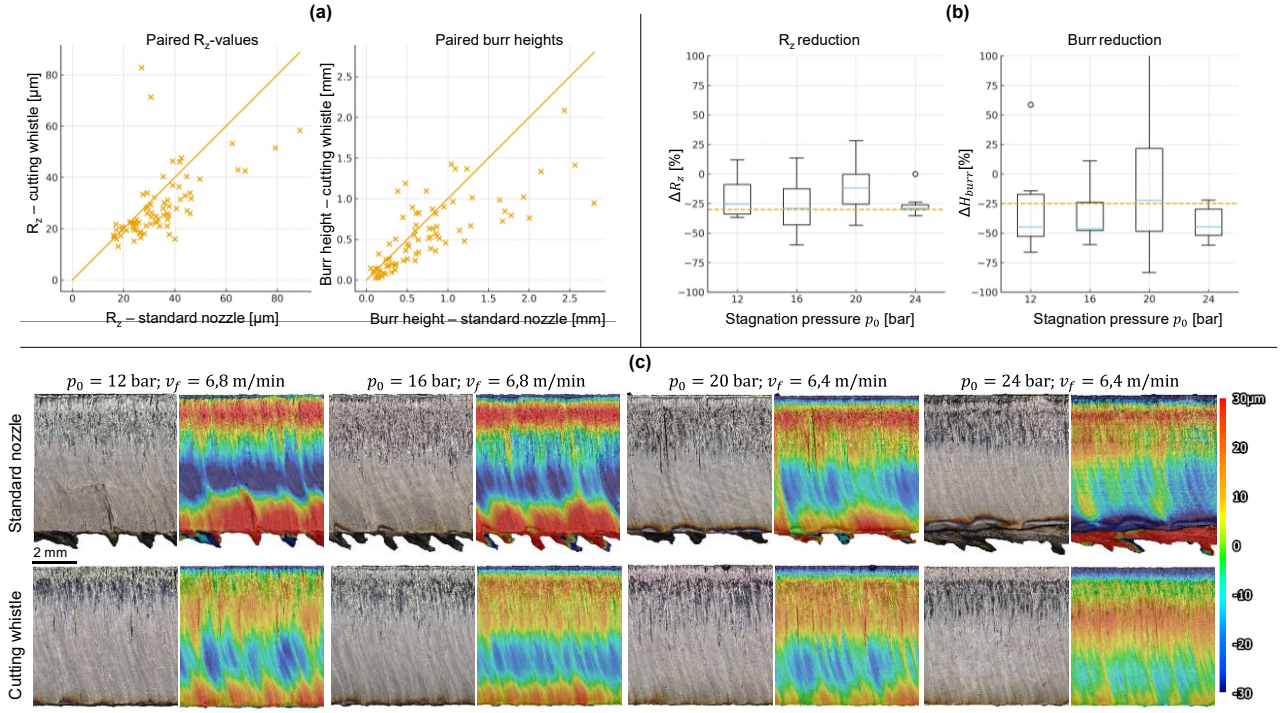

Figure 6: Quality impact under matched throughput (6 mm, $N_z = 0.7$ mm): (a) paired scatter of R_z and H_{burr} (cutting whistle vs. standard), (b) boxplots of relative changes versus p_0, and (c) representative edge images illustrating delayed burr onset with the cutting whistle.

The improvements become most pronounced within the coupling window identified earlier (sufficiently high stagnation pressure and a stand-off around $N_z \approx 0.7$ mm) and for focus settings that favor stable melt evacuation near the exit. In this regime, the cutting whistle produces an expanded "quality plateau" in terms of simultaneously low roughness and reduced burr, while moderately increasing the achievable cutting speed up to 10 %. This is consistent with the reduced framework introduced in Section 4.2: when the excitation band is depth-effective and the coupling is strong, the melt film is less prone to blocking-prone accumulation cycles near the lower front and can be evacuated more continuously. Conversely, outside this operating window—e.g., at insufficient pressure or at stand-off settings that reduce effective coupling—the quality gain becomes smaller and more variable.

Overall, the quality results support the central conclusion of this paper: temporal structuring of the gas forcing, implemented by a resonator-equipped nozzle at constant gas throughput, provides a robust pathway to reduce roughness and burr and to extend the usable process window in laser fusion cutting of austenitic stainless steels.

5 Summary

The work presented in this paper summarizes the main steps taken in subproject A08 of SFB 1120 to improve cut-edge precision in laser fusion cutting of austenitic stainless steels. Starting from industrial reference conditions with roughness values Rz of about 60–70 µm and pronounced burr at 6 mm thickness, the combination of in-situ diagnostics and targeted actuation has enabled a stepwise reduction of melt-film instabilities. In Phase 1, access to the cutting front via a transparent trimming-cut rig and high-speed imaging revealed the dominant instability mechanisms and showed that an appropriate use of beam divergence can already reduce roughness by roughly a factor of three.

In Phase 2, extending the diagnostic chain towards schlieren imaging and acoustic measurements exposed thickness-dependent resonances of the coupled gas–film system. This led to the development of a resonator-equipped nozzle that generates a geometrically fixed, narrowband aeroacoustic mode with pressure-dependent amplitude. A reduced thin-film framework links gas-side interfacial shear and streamwise pressure forcing to a film-side cut-off frequency and blocking logic and thereby guides the choice of effective modulation bands. High-speed imaging confirms a depth-dependent low-pass response of the melt film: lower and medium frequency bands couple more efficiently into the lower front, increase the time-averaged interfacial shear and suppress large-scale, low-frequency accumulation events.

Under matched gas throughput, this narrowband gas modulation leads to a robust reduction of cut-edge roughness and burr height and to a moderate increase of the maximum cutting speed. In favorable parameter windows, the achievable roughness is in the 10–20 µm range, thus approaching an order-of-magnitude improvement in surface precision, while simultaneously mitigating burr

formation. These results underline that the temporal structure of the gas field is a powerful additional design variable, complementary to beam and nozzle geometry.

Acknowledgements

The presented investigations were carried out at the Chair of Laser Technology LLT of RWTH Aachen University and Fraunhofer Institute for Laser Technology ILT within the framework of the collaborative Research Centre SFB1120-236616214 “Bauteilpräzision durch Beherrschung von Schmelze und Erstarrung in Produktionsprozessen” and funded by the Deutsche Forschungsgemeinschaft e.V. (DFG, German Research Foundation). The sponsorship and support are gratefully acknowledged.

Conflict of Interest

The author declares no conflict of interest.

Data Availability Statement

The data supporting the findings of this study are available at http://hdl.handle.net/21.11102/60822e64-6a99-4e54-9910-2bba1b0240f6.

References

[1] Petring, D.; Abels, P.; Beyer, E.; Herziger, G. (1988): Werkstoffbearbeitung mit Laserstrahlung. Teil 10: Schneiden von metallischen Werkstoffen mit CO2-Hochleistungslasern. In: Feinwerktechnik & Messtechnik 96, S. 364–372.

[2] Mahrle, Achim; Borkmann, Madlen; Pfohl, Peer (2021): Factorial Analysis of Fiber Laser Fusion Cutting of AISI 304 Stainless Steel: Evaluation of Effects on Process Performance, Kerf Geometry and Cut Edge Roughness. In: Materials (Basel, Switzerland) 14 (10). DOI: 10.3390/ma14102669.

[3] Stoyanov, S.; Petring, D.; Piedboeuf, F.; Lopes, M.; Schneider, F. (2023): Numerical and experimental investigation of the melt removal mechanism and burr formation during laser cutting of metals. In: Journal of Laser Applications 35 (4), Artikel 042028. DOI: 10.2351/7.0001182.

[4] Goppold, Cindy; Zenger, Karsten; Herwig, Patrick; Wetzig, Andreas; Mahrle, Achim; Beyer, Eckhard (2014): Experimental Analysis for Improvements of Process Efficiency and Cut Edge Quality of Fusion Cutting with 1µm Laser Radiation. In: Physics Procedia 56, S. 892–900. DOI: 10.1016/j.phpro.2014.08.108.

[5] Petring, Dirk; Molitor, Thomas; Schneider, Frank; Wolf, Norbert (2012): Diagnostics, Modeling and Simulation: Three Keys Towards Mastering the Cutting Process with Fiber, Disk and Diode Lasers. In: Physics Procedia 39, S. 186–196. DOI: 10.1016/j.phpro.2012.10.029.

[6] Arntz, D.; Petring, D.; Stoyanov, S.; Jansen, U.; Schneider, F.; Poprawe, R. (2018): In situ visualization of multiple reflections on the cut flank during laser cutting with 1 µ m wavelength. In: Journal of Laser Applications 30 (3), Artikel 032206. DOI: 10.2351/1.5040614.

[7] Arntz, D.; Petring, D.; Schneider, F.; Poprawe, R. (2019): In situ high speed diagnosis—A quantitative analysis of melt flow dynamics inside cutting kerfs during laser fusion cutting with 1 µ m wavelength. In: Journal of Laser Applications 31 (2), Artikel 022206. DOI: 10.2351/1.5096091.

[8] Arntz‐Schroeder, Dennis; Petring, Dirk (2020): Analyzing the Dynamics of the Laser Beam Cutting Process. In: PhotonicsViews 17 (2), S. 43‐47. DOI: 10.1002/phvs.202000015.

[9] Oliveira Lopes, M. de; Petring, D.; Stoyanov, S.; Gillner, A. (2023): Control of melt dynamics in laser cutting based on a resonant nozzle cavity. In: Journal of Manufacturing Processes 105, S. 399–406. DOI: 10.1016/j.jmapro.2023.09.051.

[10] Oliveira Lopes, M. de; Schneider, F.; Gillner, A.; Häfner, C. (2024): Suppression of melt flow instabilities by amplifying high-frequency melt waves in laser fusion cutting. In: Journal of Manufacturing Processes 131, S. 2255–2262. DOI: 10.1016/j.jmapro.2024.10.040.

[11] Rossiter, J. E. (1964): Wind tunnel experiments on the flow over rectangular cavities at subsonic and transonic speeds. In: *London: Aeronautical Research Council, Reports and Memoranda, Rept. 3488*. Online verfügbar unter https://reports.aerade.cranfield.ac.uk/handle/1826.2/4020.

[12] Vicanek, M.; Simon, G.; Urbassek, H. M.; Decker, I. (1987): Hydrodynamical instability of melt flow in laser cutting. In: J. Phys. D: Appl. Phys. 20 (1), S. 140–145. DOI: 10.1088/0022-3727/20/1/021.

[13] Borkmann, Madlen; Mahrle, Achim; Wetzig, Andreas (2023): Laser fusion cutting: The missing link between gas dynamics and cut edge topography. In: Journal of Laser Applications 35 (4), Artikel 042017. DOI: 10.2351/7.0001103.

[14] Schlichting, Hermann; Gersten, Klaus (2017): Fundamentals of Boundary–Layer Theory. In: Hermann Schlichting und Klaus Gersten (Hg.): Boundary-Layer Theory. Berlin, Heidelberg: Springer Berlin Heidelberg, S. 29–49. DOI: 10.1007/978-3-662-52919-5_2.

[15] Tennekes, H. and Lumley, J.L. (1972): A First Course in Turbulence. Cambridge, Massa-chusetts, and London, England: The MIT Press.